Infrared Measurements Throughout Polar Night using Two AERIs in the Arctic

Z. Mariani*[1], K. Strong[1], M. Wolff[1, 2], P. Rowe[3], V. Walden[3], P. F. Fogal[1, 4], T. Duck[5], G. Lesins[5], D. S. Turner[6], C. Cox[3], E. Eloranta[7], J. R. Drummond[5], C. Roy[8], R. L. Lachance[8], D. D. Turner [9], D. Hudak[4], I.A. Lindenmaier[1, 10]

[1] Department of Physics, University of Toronto, Toronto, ON, Canada
[2] The Norwegian Meteorological Institute, Oslo, Norway
[3] Department of Geography, University of Idaho, Idaho, USA
[4] Air Quality Research Division, Environment Canada, Downsview, Canada
[5] Department of Physics, Dalhousie University, Halifax, NS, Canada
[6] Data Assimilation and Satellite Meteorology Research Section, Env. Canada, Downsview, ON, Canada
[7] University of Wisconsin Space Science and Engineering Centre, Madison, Wisconsin, USA
[8] ABB, Quebec City, Canada
[9] NOAA / National Severe Storms Laboratory, Norman, Oklahoma, USA
[10] Thunder Bay Regional Research Institute, Thunder Bay, ON, Canada

ABSTRACT

The Extended-range Atmospheric Emitted Radiance Interferometer (E-AERI) is a moderate resolution (1 cm^{-1}) Fourier transform infrared spectrometer for measuring the absolute downwelling infrared spectral radiance from the atmosphere between 400 and 3000 cm^{-1}. The extended spectral range of the instrument permits monitoring of the 400–550 cm^{-1} (20–25 μm) region, where much of the infrared surface cooling currently occurs in the dry air of the Arctic. The E-AERI provides information about radiative balance, trace gases, and cloud properties in the Canadian high Arctic. The instrument was installed at the Polar Environment Atmospheric Research Laboratory (PEARL) Ridge Lab at Eureka, Nunavut, in October 2008. Measurements are taken every seven minutes year-round (precipitation permitting), including polar night when the solar-viewing spectrometers are not operated. A similar instrument, the University of Idaho's Polar AERI (P-AERI), was installed at the Zero-altitude PEARL Auxiliary Laboratory (0PAL), 15 km away from the Ridge Lab, from March 2006 to June 2009. During the period of overlap, these two instruments provided calibrated radiance measurements from two different altitudes.

Retrievals of total columns of various trace gases are being evaluated using a prototype version of the retrieval algorithm SFIT2 modified to analyze emission features. In contrast to solar absorption measurements of atmospheric trace gases, which depend on sunlit clear-sky conditions, the use of emission spectra allows measurements year-round (except during precipitation events or when clouds are present). This capability allows the E-AERI to provide temporal coverage throughout the four months of polar night and to measure the radiative budget throughout the entire year. This presentation will describe the new E-AERI instrument, its performance evaluations, and clear sky vs. cloudy measurements.

Keywords: Remote sensing, Arctic atmospheric measurements, trace gas retrievals, Fourier transform infrared spectrometer (FTIR), AERI, emission spectra, radiative balance, total column measurements

1. INTRODUCTION

The Canadian Network for the Detection of Atmospheric Change (CANDAC) has equipped the Polar Environment Atmospheric Research Laboratory (PEARL) at an altitude of 610 m at Eureka, Nunavut (80ºN, 86ºW) for measurements during International Polar Year (IPY, project 196) and beyond. One of the instruments at PEARL is the Extended-range Atmospheric Emitted Radiance Interferometer (the E-AERI). This instrument measures the absolute downwelling infrared radiation spectrum for studies of the Arctic radiation budget and atmospheric composition. The E-AERI was installed in October 2008 and acquired one full year of measurements at the PEARL Ridge Lab independent of sunlight, which is beneficial in the Arctic due to prolonged periods without sunlight during polar night.

Remote Sensing of Clouds and the Atmosphere XVII; and Lidar Technologies, Techniques, and Measurements for Atmospheric Remote Sensing VIII, edited by Evgueni I. Kassianov, Adolfo Comeron, Richard H. Picard, Klaus Schäfer, Upendra N. Singh, Gelsomina Pappalardo, Proc. of SPIE Vol. 8534, 85340H · © 2012 SPIE · CCC code: 0277-786/12/$18 ·

The University of Wisconsin Space Science and Engineering Centre (UW-SSEC) developed the first AERI, and has since deployed several others to dedicated sites in the Southern Great Plains, the North Slope of Alaska, and the Tropical Western Pacific [Stokes and Schwartz, 1994]. The E-AERI is an expansion on the original AERI design, extending beyond the spectral coverage range of a standard AERI from 550–3000 to 400–3000 cm^{-1}. Details of the instrument's certification, calibration, and setup are provided in Mariani *et al.* [2012]. A previous extended-range version of the AERI system was deployed at the ARM Surface Heat Budget of the Arctic Ocean Ice Station in 1997 to investigate the far infrared H_2O continuum [Tobin *et al.*, 1999]; the ARM program has also operated an extended range AERI at its North Slope of Alaska site since 1999 that has been used in a wide range of research [e.g., Delamere et al 2010, Turner and Eloranta 2008, Lubin and Vogelmann 2006].

The E-AERI was constructed by ABB under commercial license from UW-SSEC and incorporates the newest generation of ABB's FTIR spectroradiometer, UW-SSEC blackbody cavity, latest COTS signal conditioning units, and new detector/Stirling cooler with extended lifetime. The new configuration allows in-field replacement of the Stirling cooler and metrology laser. The software has been updated with a combination of ABB software for data acquisition and instrument communication/control interface and UW-SSEC software for post-processing and atmospheric science functions to ease future evolution of hardware and software by each party (ABB and UW-SSEC). This new generation of AERIs also includes updated protective enclosures against atmospheric precipitation and interferometer temperature variation.

The sampling interval of approximately seven minutes allows the study of short-term meteorological phenomena in the lower atmosphere, e.g., inversion developments, cloud effects, and front passages [Turner et al., 2000]. The spectral range of the E-AERI has been extended to cover the so-called dirty window (around 400 cm^{-1}, or 25 μm), where much of the infrared cooling currently occurs in the dry air of the Arctic. Due to climate change, the water vapour content in the Arctic atmosphere is expected to increase, which would result in a change of the radiative transfer. Such a regime shift should be visible in the E-AERI data record. The installation of the E-AERI at PEARL was preceded by the University of Idaho's Polar-AERI (P-AERI), which was deployed at the Zero-altitude PEARL Auxiliary Laboratory (0PAL) from March 2006, to June 2009 [Walden et al., 2005, Rowe et al., 2008]. The location of these two measurement sites are shown in Figure 1. The two instruments are similar, but the P-AERI does not provide spectral coverage below 550 cm^{-1}.

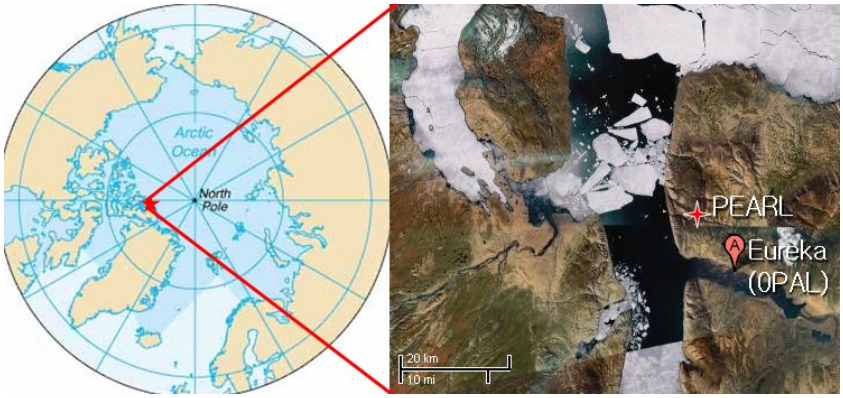

Figure 1: Location of the two measurement sites at Eureka, Nunavut, Canada.
Image: CIA World Factbook, Google Maps.

Retrievals of total columns of various trace gases (e.g. CH_4, CO, CO_2, O_3, N_2O) using a prototype version of the retrieval algorithm SFIT2 [Pougatchev *et al.*, 1995], modified to use emission features within the measured wavelength range, are currently being evaluated. Recently, retrievals of CO with high sensitivity to the lower troposphere have been demonstrated for the AERI systems [Yurganov *et al.*, 2010]. In contrast to solar absorption measurements of atmospheric trace gases, which depend on sunlit clear-sky conditions, the use of emission spectra allows measurements year-round. This capability allows the E-AERI to extend the temporal coverage of other ground-based spectrometers at PEARL throughout the polar night.

* ZMariani@atmosp.physics.utoronto.ca; phone (416) 946-0869; U. of Toronto, Dept. Physics, 60 St. George Street, Toronto

2. INSTRUMENT DESIGN

The E-AERI is composed of three distinct parts: (1) the front-end optics, (2) the back-end electronics and interferometer, and (3) the computer (standard off-the-shelf laptop). The front-end optics consists of two blackbodies and the scene mirror. The scene mirror has a gold reflecting surface and is mounted at 45° to the motor rotation axis, which is in turn positioned coincident with the interferometer input optical axis. This configuration allows different views: nadir, zenith, Ambient Blackbody (AB) and Hot Blackbody (HB).

The E-AERI measures emission from the atmosphere using an MR-300 series Fourier Transform Spectrometer (FTS) calibrated with the two blackbodies. One measurement cycle includes a zenith-sky measurement as well as calibration measurements of two internal blackbodies to ensure accurately calibrated zenith-sky spectra. The main component of the back-end electronics is the Michelson interferometer with computer interface. The maximum optical path difference is 1 cm, providing an unapodized resolution of 1 cm^{-1}. Two IR detecting channels are supported by an extended-range mercury cadmium telluride (MCT) detector coupled with a photovoltaic indium antimonide (InSb) detector mounted in a sandwich configuration. The detectors are housed in a dewar and cooled below 70 K by a linear Stirling-cycle cryo-cooler. The back-end components' temperatures are kept stable through the temperature control unit attached to the back-end electronics. Electronic modules are also mounted in the back-end: the signal conditioning electronics, blackbody temperature controller, and Stirling cooler support electronics.

The instrument is designed to be configured as stand-alone or mounted thru-wall. Figure 2 illustrates the interior of the front-end of the E-AERI in the thru-wall configuration, as installed at PEARL. The performance characteristics of the E-AERI are summarized in Table 1. Items with a '*' indicate performance metrics verified during calibration at UW-SSEC.

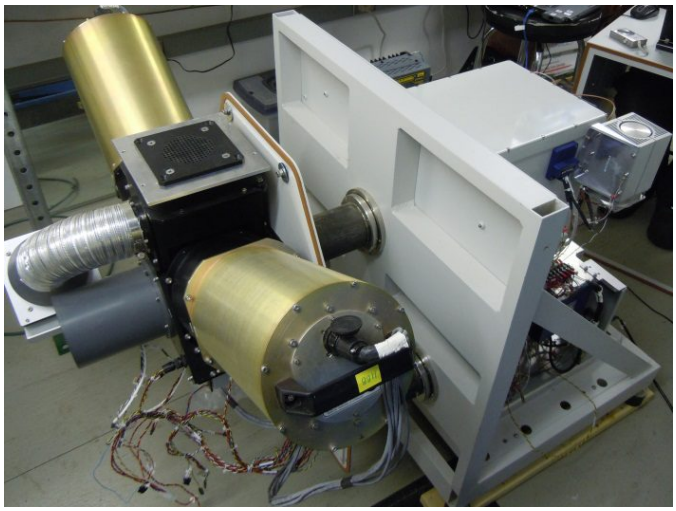

Figure 2: The E-AERI during installation at PEARL with the front- and back-end enclosures removed. The back-end of the instrument (partially hidden) houses the interferometer.

Measurements of the emission from the two blackbodies are used to calibrate the sky-view measurement. The two calibration blackbodies are of identical construction, each consisting of a thermally isolated cavity that is painted with a high-emissivity diffuse black paint. Each blackbody's temperature can be set using the instrument's software. For operation at PEARL, the HB is set at 310 K and the AB operates at the outside temperature. The approach used for radiometric calibration of the E-AERI system is based on that of Revercomb et al. [1988].

Three vignetting mapping tests were performed on the zenith-sky, HB, and AB views to verify the optical alignment of the source and reference blackbody cavities. Figure 3 illustrates the field-of-view mapping for the HB. All values on the periphery are zero, indicating that the field-of-view has a clear path to the HB. Similar results were obtained for the zenith-sky and AB tests.

Table 1: E-AERI instrument performance.

Item	Performance
General System Elements	• ABB Bomem MR-300 Michelson interferometer with PC computer interface • Full-aperture temperature-controlled calibration reference sources • Automated system for providing sequential views of the sky (zenith) and two blackbodies (one at ambient temperature, one at 37°C) for radiometric calibration • Environmental Monitoring System, for blackbody temperature data • Computer and Data Handling System, for sequencing all E-AERI operations and data handling, including acquisition, processing, display, and networking
*Spectral range	400–3000 cm^{-1} (3.3–25 μm)
*Spectral resolution	1.0 cm^{-1}, unapodized maximum optical path difference [OPD] of 1 cm
*Spatial and angular FOV	46 ±1 mrad full angle
*Radiometric calibration absolute accuracy	< 1% of ambient blackbody radiance
*Reproducibility	< 0.2% of ambient blackbody radiance
*Blackbody cavity characterization	• Temperature Knowledge: ±0.1°C of absolute temperature • Emissivity knowledge: better than ±0.1% • Temperature stability: better than 0.05°C over viewing period (» 120 s)
*Nonlinearity knowledge	Better than 0.1%
*Polarization	< 0.1%
*Wavelength calibration	Channel wavenumber knowledge: better than 0.01 cm^{-1}
*Noise (RMS for 2-min blackbody view)	< 0.4 mW (m^2 sr cm^{-1})$^{-1}$ for 420–1400 cm^{-1} (except 667 cm^{-1}, where CO_2 in the instrument reduces responsivity) <0.015 mW (m^2 sr cm^{-1})$^{-1}$ for 2000–2600 cm^{-1} (except 2300–2400 cm^{-1}, where CO_2 in the instrument reduces responsivity)
Temporal sampling	Repeat cycle: ≈ 7 min Interferometer scan period: < 2 s
Detectors	Two detectors are mounted in sandwich configuration covering two spectral regions: Channel one (400–1800 cm^{-1}): extended-range photoconductive mercury cadmium telluride (MCT) Channel two (1800–3000 cm^{-1}): photovoltaic indium antimonide (InSb)
Beamsplitter	Potassium bromide (KBr)
Operational requirement	Automatic control system hardware contains these features: • Scheduled sequencing of the following operations: – Scene switching between sky and blackbody views – Interferometer and housekeeping data acquisition and transfer • Capability of remotely changing the operation listed above • 24-hour continuous operations with data output at 7-min intervals • Linear stirling-cycle cryo-cooler keeps detectors cooled down below 70 K • Real-time display with flags for out-of-limit conditions
Operating environment	Operating temperature: • Spectroradiometer (back-end) enclosure: −30° to +40°C • Input and calibration (front-end) enclosure: −70° to +40°C
Data products	Primary (required for scientific use): • Calibrated spectra • Standard deviation for blackbody and sky views • Calibration coefficient and blackbody temperature Secondary (auxiliary information for real-time monitoring and quality control): • Ambient air temperature • Ambient pressure • Ambient humidity • Instrument housekeeping data

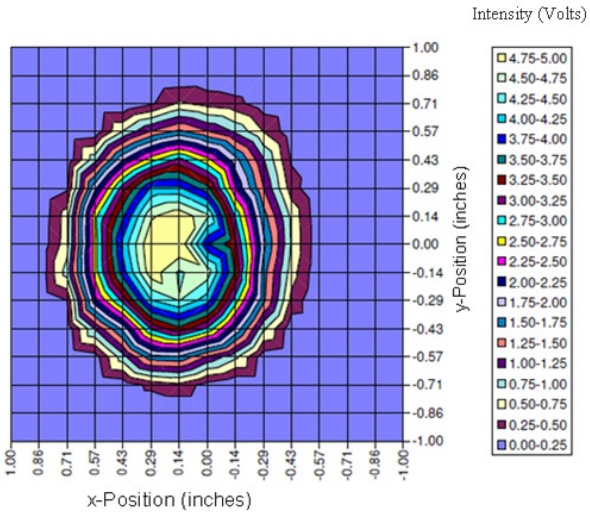

Figure 3: Typical radiometric field-of-view mapping of the aperture of the E-AERI HB. Values around the periphery are zero, verifying optical alignment. Similar results are obtained for the AB and zenith-sky field-of-view. Figure: ABB.

3. INSTRUMENT PERFORMANCE

The E-AERI was sent to UW-SSEC for calibration and performance evaluation from September to October 2008 and met the requirements for Noise Equivalent Spectral Radiance (NESR) and radiometric calibration [Mariani *et al.*, 2012]. A side-by-side comparison with two UW-developed AERI systems, the AERI-07 (with extended-range detector) and AERI-Bago, was performed. These instruments have been employed in numerous measurement campaigns and are considered reliable benchmarks for measurement inter-comparison purposes [Knuteson *et al.,* 2004a]. Results from these comparisons indicate strong agreement between the instruments, verifying the accuracy of the E-AERI's spectra [UW-SSEC, 2008].

Another side-by-side comparison was performed on October 20, 2008 in Eureka with the previously-installed P-AERI at 0PAL. Excellent agreement was found between these two instruments, with the exception of the 1450–1800 cm^{-1} region. Spikes are visible in the E-AERI (but not P-AERI) spectra in this region as shown in Figure 4. Each spike in the NESR has a corresponding water line in the water lines spectrum. Figure 4 [Right] is a similar radiance measurement taken by the E-AERI several months later on 4 April 2009 at PEARL. Hence the October 20 spectrum was recorded before the instrument had time to dry out – it took ~ 8 days for the instrument to dry out to a point where the spikes were not detectable.

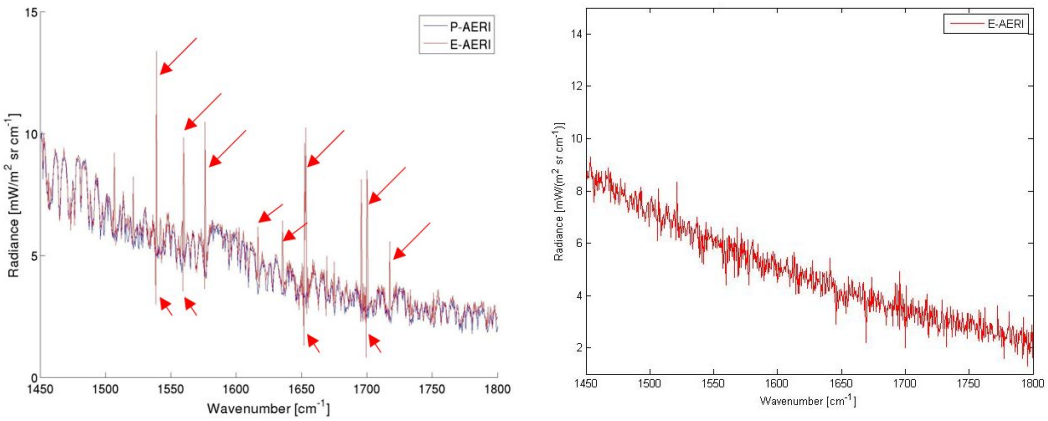

Figure 4: Measured radiance in the 1450–1800 cm^{-1} region on 20 October 2008 [Left] and 4 April 2009 [Right]. Spikes in the E-AERI observations (red arrows) do not exist in the P-AERI spectra due to a lack of humidity in the P-AERI. The complete absence of such spikes in the E-AERI spectra is observed several months later once the instrument had time to dry out [Right].

The ability of the E-AERI to operate independent of sunlight provides excellent temporal coverage in a region that experiences prolonged periods of darkness (i.e. polar night). The radiance measured by the E-AERI for the last half of April 2009 is shown in Figure 5. An increase in radiance, particularly in the 750–1400 cm^{-1} region, as clouds pass overhead is observed. The diurnal change in temperature can also be observed in the 600–800 cm^{-1} CO_2 band, which is highly temperature-dependent. The additional presence of water vapour in cloud formations increases water vapour emission in the E-AERI's spectra. For instance, an increase in radiance in the 750–1400 cm^{-1} cloud-sensitive region on April 16 is observed in the morning due to thin clouds, followed by a sudden return to lower clear-sky radiances at ~24:00 (UTC) as the cloud front passes Eureka.

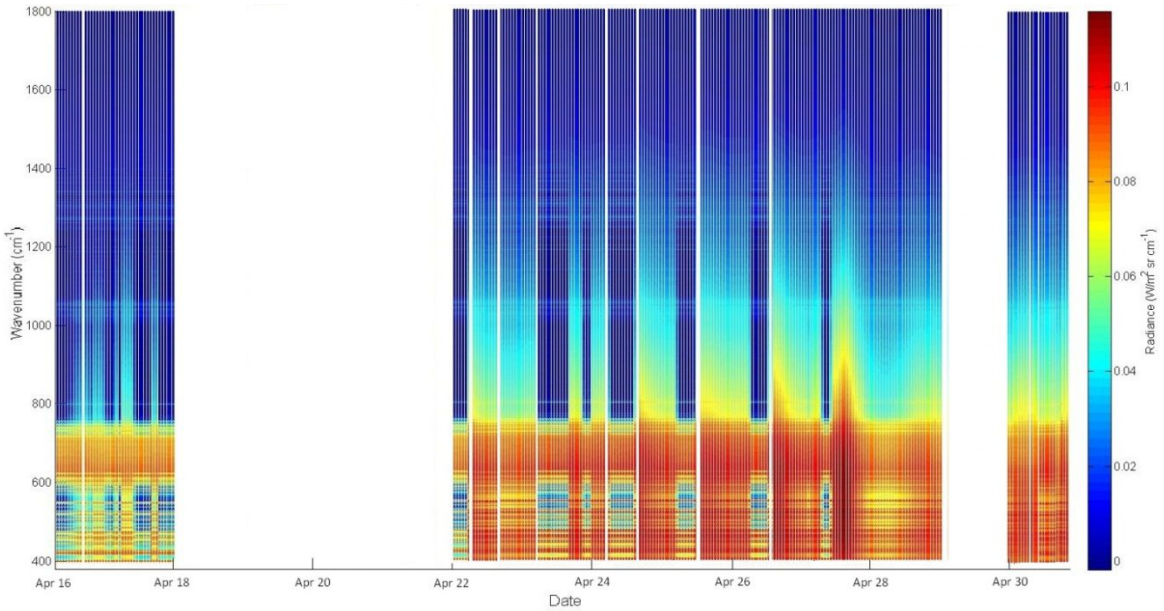

Figure 5: E-AERI radiance measurements from April 16-30, 2009. Only the longwave spectral region is shown (up to 1800 cm^{-1}) for clarity. White spaces correspond to periods with no measurements (precipitation, instrument maintenance).

Comparisons between the E-AERI (at PEARL) and the P-AERI (at 0PAL) measurements of radiance at 00:08 UTC on 4 April 2009 are shown in Figure 6 (a). Differences in each instrument's spectrum correspond to differences in the measurement site's temperature and humidity. 4 April 2009 radiances were simulated using a Fast Line By Line (FLBL) radiative transfer model for an altitude of 10 m (P-AERI) and 610 m (E-AERI). The radiances are computed for clear skies with no aerosols (4 April 2009 had clear skies throughout the day). Radiosonde and ozone soundings were interpolated and included in the simulation. Results from the model simulations are shown in Figure 6 (b). Residuals from the measured spectra (a) and simulated spectra (b) are shown in Figure 6 (c) and indicate strong agreement between the simulated and observed radiances, with the exception of the boundaries around the 600–800 cm^{-1} CO_2 region and around the 1600–1800 cm^{-1} region. Model simulations indicate that the simulated radiances are very sensitive to changes in temperature and water vapour in the lowest 3 km of the atmosphere. Radiosonde water vapour profiles errors (10–20%) and temperature errors (< 2 K) result in the emission and absorption features to become saturated and a baseline shift in the simulated radiances. Hence this demonstrates the reliance on accurate radiosonde profiles for simulated radiances. These comparisons provide insight into the first 600 m of the atmosphere above Eureka and permit a direct comparison between the radiative budgets measured at the two locations.

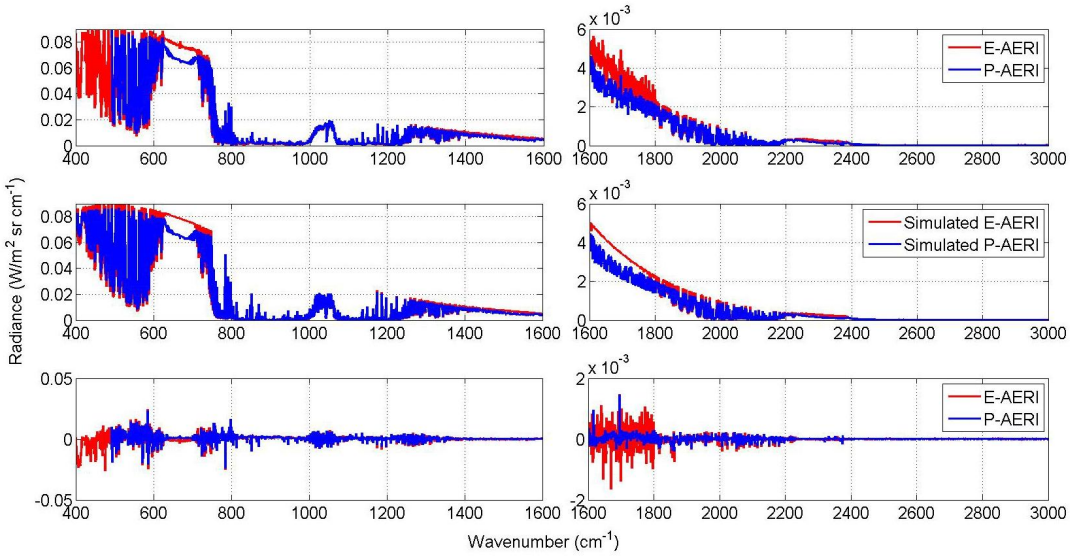

Figure 6: (a) E-AERI (red) and P-AERI (blue) measured radiances at 00:08 (UTC) on 4 April 2009 with (b) simulated spectra shown below. (c) Differences between the measured and simulated spectra for each instrument (a – b).

4. CLEAR SKY VS. CLOUDY MEASUREMENTS

The ability of AERI systems to detect the presence of clouds and analyze cloud properties has been well demonstrated [DeSlover *et al.*, 1999; Collard *et al.*, 1995; Shaw *et al.*, 2005; and Turner *et al.*, 2005]. The Millimeter Wave Cloud Radar (MMCR) installed at 0PAL provides cloud heights, thicknesses, internal structure and vertical motions with high temporal (2 s) and vertical resolution. 16 April 2009 was selected as a day for comparison because of early-morning clear skies followed by the presence of a thick cloud layer above Eureka for the remainder of the afternoon and evening, as detected by the MMCR [Mariani *et al.*, 2012]. As shown in Figure 7, the E-AERI's measured radiance and brightness temperature increases in the afternoon primarily in the 400–600 cm^{-1} and 750–1400 cm^{-1} regions due to the emission by additional water vapour/liquid/ice, correlating with the MMCR's detection of a low-altitude cloud layer at this time. These increases are several times larger than for more southern latitudes; thus the impact of clouds on the radiation budget is greater in the Arctic than in other more humid regions due to the atmospheric window being more transparent. Such large increases in radiance in these spectral regions provide a means to detect cloud cover using E-AERI spectra.

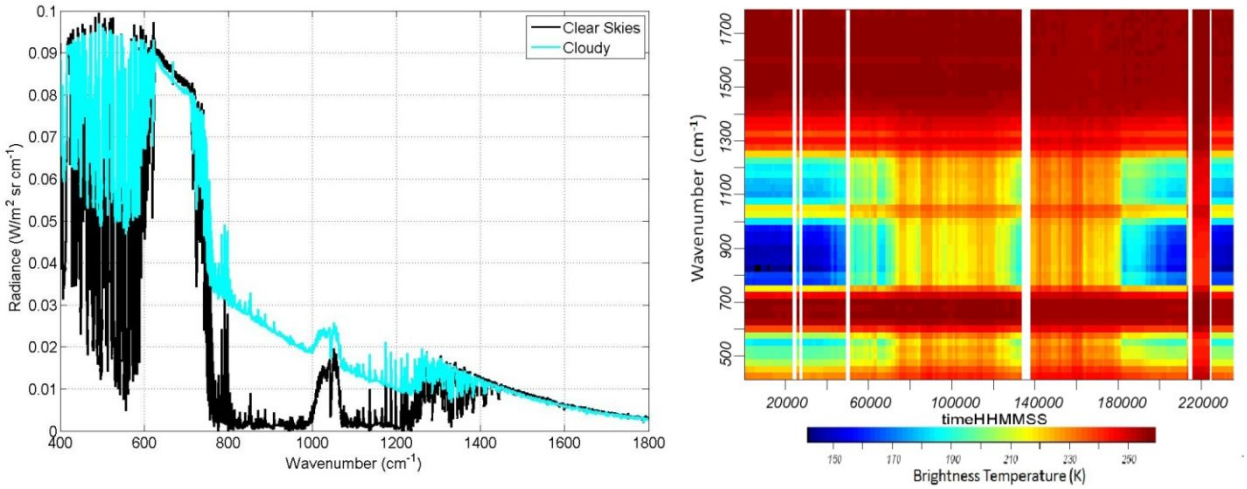

Figure 7: Left: Averaged E-AERI measurements of radiance on 16 April 2009 from 00:00-01:00 UTC (cyan) and 17:00–18:00 UTC (black). Right: Brightness temperatures measured throughout 16 April 2009.

A low-level ice crystal cloud was present on April 5, 2009, as reported throughout the day by a meteorological technician at the Eureka weather station and detected by the MMCR and Arctic High Spectral Resolution LIDAR instruments [Mariani *et al.*, 2012]. A 10-minute interval (20:30–20:40 UTC) was selected from this day since the ice crystals were concentrated below the E-AERI (610 m) at this time, providing a unique opportunity to assess their impact on the radiative budget at two altitudes. Ice crystal radiances were compared to clear-sky radiances measured the day before (April 4, 2009) at 0:08–00:18 UTC. Radiance measurements made during these two ten-minute time intervals were averaged, and both instruments' differences (ice – clear) are shown in Figure 8. The P-AERI measured the largest increases in radiance since it was located below the ice crystal cloud and received emission from the ice particles.

Longwave downwelling radiances during the April 5 case were converted to longwave downwelling all-sky irradiance based on the method of Cox et al. [2012]. The longwave downwelling irradiance from the ice crystal cloud was found to be 7.8 ±2 W m^{-2} (5 W m^{-2} greater than measured by the E-AERI). This is equivalent to a 6% ±1% increase in longwave downwelling irradiance from the ice crystal cloud measured by the P-AERI (located below the cloud). A 6% irradiance increase for this ~600-m thick cloud is in agreement with the measured surface forcing of up to 36% irradiance from thicker ice clouds (> 2 km) found in Lesins et al. [2009]. Given the frequency of ice crystal events at Eureka, this can have important consequences for the surface energy balance in the Arctic region.

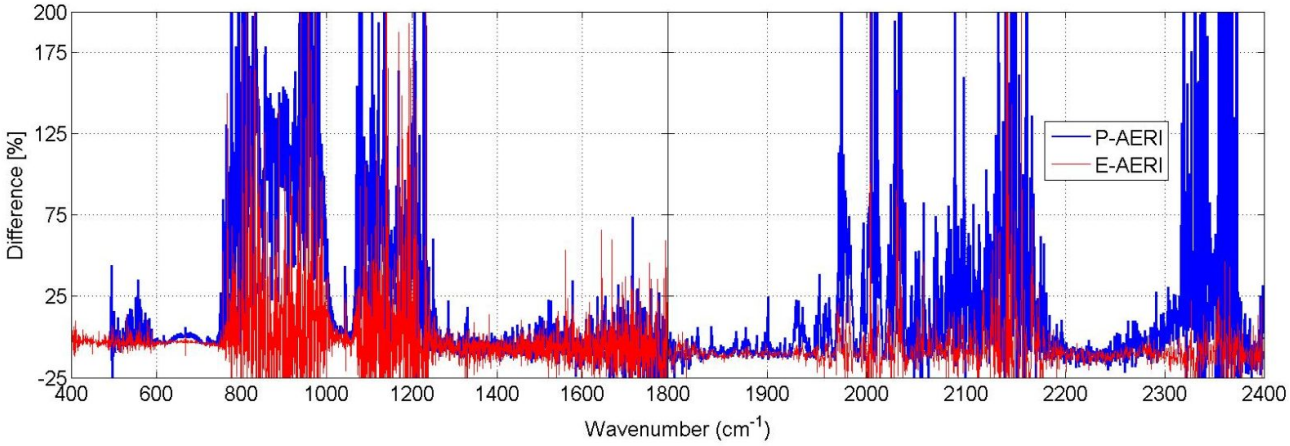

Figure 8: Percent difference between the ice crystal and clear-sky radiances (ice-crystal – clear sky/clear sky). Differences for the E-AERI (red) and P-AERI (blue) radiances are shown for clear skies on 4 April 2009 (00:08–00:18 UTC) and the ice-cloud on 5 April 2009 (20:30–20:40 UTC).

5. CONCLUSION

The E-AERI instrument was calibrated and passed certification testing at the UW-SSEC in September 2008. One full year of data (throughout polar night) were acquired with the E-AERI after its installation at PEARL in October 2008. In September 2009 the E-AERI was moved to 0PAL; measurements from an altitude of 10 m continue to be taken to determine concentrations of tropospheric trace gases and investigate infrared cooling in the 25 μm region. E-AERI radiance measurements have been extensively validated and show excellent agreement in side-by-side measurement comparisons with several different AERI systems. The radiative impact of clouds has been measured, showing a strong increase in radiance, particularly in the 750–1400 cm^{-1} region, which incurs > 100% increase in downwelling radiance on average. This increase is several times greater in the Arctic than for more southern latitudes. A 6% increase in irradiance was measured from a thin low-level ice cloud, which is in good agreement with previous studies. Retrievals of trace gases, such as O_3, CO, CH_4, N_2O, etc., are currently being evaluated using a new emission version of the SFIT2 retrieval code. Obtaining total columns of various trace gases will provide insight into the atmospheric composition above Eureka throughout polar night. The E-AERI observations will provide a climatology of the infrared radiation budget and total columns of trace gases.

6. ACKNOWLEDGEMENTS

PEARL is operated by CANDAC. CANDAC/PEARL funding partners are: the Arctic Research Infrastructure Fund, Atlantic Innovation Fund/Nova Scotia Research Innovation Trust, Canadian Foundation for Climate and Atmospheric Science, Canada Foundation for Innovation, Canadian Space Agency (CSA), Environment Canada (EC), Government of Canada International Polar Year, Natural Sciences and Engineering Research Council (NSERC), Ontario Innovation Trust, Ontario Research Fund, Indian and Northern Affairs Canada, and the Polar Continental Shelf Program. Spring visits to PEARL were made as part of the Canadian Arctic ACE Validation Campaigns, led by Kaley A. Walker and supported by CSA, EC, NSERC and the Northern Student Training Program. Thanks to CANDAC operators Ashley Harrett, Alexei Khmel, Paul Loewen, Oleg Mikhailov, Keith MacQuarrie and Matt Okraszewski who have helped with the P-AERI and E-AERI measurements at PEARL. Thanks to Stéphane Lantagne from ABB Bomem for his work installing the E-AERI at PEARL. Thanks also to the staff at the Eureka Weather Station for their support and hospitality.

REFERENCES

Collard, A.D., S.A. Ackerman, W.L. Smith, H.E. Ma, H.E. Revercomb, R.O. Knuteson, and S.C. Lee (1995): Cirrus cloud properties derived from high spectral resolution infrared spectrometry during FIRE II. Part III: Ground-based HIS results. *J. Atmos. Sci.*, 52, 4264–4275.

Cox, C., V. Walden, and P. Rowe (2012): A comparison of the atmospheric conditions at Barrow, Alaska and Eureka, Canada (2006–2008). *J. Geophys. Res.*, 117, D12204.

Delamare, J. S., S. A. Clough, V. Payne, E. J. Milawer, D. D. Turner, R. R. Gamache (2010): A far-infrared radiative closure study in the Arctic: Application to water vapor. *J. Geophys. Res.*, 115, D17106.

DeSlover, D. H., Smith, W. L., Piironen, P. K., and Eloranta, E. W. (1999): A methodology for measuring cirrus cloud visible-to-infrared spectral optical depth ratios. *J. Atmos. Ocean. Tech.*, 16(2), 251–262.

Knuteson, R., H. Revercomb, F. Best, N. Ciganovich, R. Dedecker, T. Dirkx, S. Ellington, W. Feltz, R. Garcia, H. Howell, W. Smith, J. Short and D. Tobin (2004a): Atmospheric Emitted Radiance Interferometer. Part I: Instrument Design. J. Atmos. Oceanic Tech., 21, 1763–1776.

Lesins, G., L. Bourdages, T. Duck, J. Drummond, E. Eloranta, V. Walden (2009): Large surface radiative forcing from topographic blowing snow residuals measured in the High Arctic at Eureka. *Atmos. Chem. Phys.,* 9, 1847–1862.

Lubin, D. and Vogelmann, A. (2006): A climatologically significant aerosol longwave indirect effect in the Arctic. *Nature*, 439, 453–456.

Mariani, Z., K. Strong, M. Wolff, P. Rowe, V. Walden, P. F. Fogal, T. Duck, G. Lesins, D. S. Turner, C. Cox, E. Eloranta, J. R. Drummond, C. Roy, D. D. Turner, D. Hudak, and I. A. Lindenmaier (2012): Infrared Measurements in the Arctic using Two Atmospheric Emitted Radiance Interferometers. *Atmos. Meas. Tech.*, **5**, 329–344.

Pougatchev, N., B. Connor, and C. Rinsland (1995): Infrared measurements of the ozone vertical distribution above Kitt Peak. *J. Geophys. Res.,* 100(D8) 16689–16697.

Revercomb, H., H. Buijs, H. Howell, D. LaPorte, W. Smith, L. Sromovsky (1988): Radiometric calibration of IR Fourier transform spectrometers: Solution to a problem with the High-Resolution Interferometer Sounder. *Appl. Opt.*, 27, 3210–3218.

Rowe, P., L. Miloshevich, D. Turner, and V. Walden (2008): Quantification of a dry bias in radiosonde humidity profiles over Antarctica. *J. Atmos. Ocean. Tech.*, 25, 1529–1541.

Shaw, J., Nugent, P., Pust, N., Thurairajah, B., Mizutani, K. (2005): Radiometric cloud imaging with an uncooled microbolometer thermal infrared camera. Opt. Express, 13(15), 5807–5817.

Stokes, G.M. and S.E. Schwartz (1994): The Atmospheric Radiation Measurement (ARM) Program: Programmatic background and design of the Cloud and Radiation Testbed. *Bull. Amer. Meteorol. Soc.*, 75, 1201–1221.

Tobin, D., F. Best, P. Brown, S. Clough, R. Dedecker, R. Ellingson, R. Garcia, H. Howell, R. Knuteson, E. Mlawer, H. Revercomb, J. Short, P. van Delst, and V. Walden (1999): Downwelling spectral radiance observations at the SHEBA ice station: Water vapor continuum measurements from 17 to 26μm. *J. Geophys. Res.,* 104(D2), 2081–2092.

Turner, D. D., Feltz, W. F., and Ferrare, R. A. (2000): Continuous water vapor profiles from operational ground-based active and passive remote sensors. *Bull. Amer. Meteorol. Soc.*, 81, 1301–1317.

Turner, D.D. (2005): Arctic mixed-phase cloud properties from AERI-lidar observations: Algorithm and results from SHEBA. *J. Appl. Meteor.*, 44, 427–444.

Turner, D. D. and E. W. Eloranta (2008): Validating Mixed-Phase Cloud Optical Depth Retrieved From Infrared Observations With High Spectral Resolution Lidar, *IEEE Geoscience and Remote Sensing Letters*, 5, 285–288.

UW-SSEC (2008): UW Final Report on ABB-Bomem E-AERI-001; Certification Testing, University of Wisconsin, December 9, 2008, 12 pp.

Walden, V.P., M. Town, B. Halter, and J. Storey (2005): First measurements of the infrared sky brightness at Dome C, Antarctica. *Publ. Astron. Soc. Pac.*, 117 (829), 300–308.

Yurganov, L., W. McMillan, C. Wilson, M. Fischer, S. Biraud, and C. Sweeney (2010): Carbon monoxide mixing ratios over Oklahoma between 2002 and 2009 retrieved from Atmospheric Emitted Radiance Interferometer spectra. *Atmos. Meas. Tech.*, 3, 1319–1331.